Physical Theory Hysteretic Model for Steel Braces

Murat Dicleli[1] and Ertugrul Emre Calik[2]

Abstract: This paper presents a simple yet efficient physical theory model that can be used to simulate the inelastic cyclic axial force–axial deformation and axial force–transverse deformation relationships of steel braces. The model consists of a brace idealized as a pin ended member with a plastic hinge located at its midlength. Input parameters of the model are based only on the properties of the brace. The model combines analytical formulations based on the nonlinear behavior of the brace with some semiempirical normalized formulas developed on the basis of a study of available experimental data. The model realistically accounts for growth effect and degradation of buckling capacity due to Baushinger effects and residual kink present within the brace and it is broadly applicable to steel braces with various section types and slenderness ratios. It is observed that the analytically obtained axial force versus axial displacement as well as axial force versus transverse displacement hysteresis loops compare reasonably well with the experimental ones.

DOI: 10.1061/(ASCE)0733-9445(2008)134:7(1215)

CE Database subject headings: Analytical techniques; Bracing; Buckling; Cyclic loads; Inelasticity; Steel; Seismic analysis.

Introduction

The most common form of seismic resistant construction of steel structures is based on ductile design, where the seismic energy during an earthquake is dissipated due to inelastic deformation of certain structural members. In the case of braced frames, the seismic energy is mainly dissipated within the braces. Thus, the overall performance of a braced steel frame depends largely on the hysteretic behavior of the braces. The hysteretic behavior of steel braces involves complex physical phenomena such as yielding in tension, progressive lengthening of the brace called growth effect, inelastic buckling in compression, as well as deterioration of the buckling capacity due to Bauschinger effect, and the residual kink that may be present within the brace. It is important to have an accurate analytical model of this complex hysteretic behavior to correctly predict the seismic response of steel braced frames particularly for performance-based design purposes.

Many experimental and analytical studies have been conducted on the hysteretic behavior of steel braces. The experimental studies of Sherman and Erzurumlu (1976), Wakabayashi et al. (1977), Jain et al. (1978), Zayas et al. (1980), Black et al. (1980), Astaneh-Asl and Goel (1984), Boutros (1999), Elchalakani et al. (2003), Shaback and Brown (2003), and Goggins et al. (2006) provided useful information on the effect of several properties of the braces on their cyclic inelastic response. In general, it was found that the slenderness ratio, end constraints, section shape, and the width-to-thickness ratios of the steel plates constituting the brace section are important parameters affecting the hysteretic behavior of the braces. Particularly, the experimental studies of Black et al. (1980) provided a wide range of data, which have been used by many researchers to develop analytical models to simulate the hysteretic behavior of braces under severe cyclic load reversals. The developed analytical models can be categorized in three groups: Finite element, phenomenological, and physical theory (Ikeda and Mahin 1984). Finite element models subdivide the brace longitudinally into a number of elements where the geometry and material properties of each element are defined. Models of this type have been used by Fujimoto et al. (1972), Kayvani and Barzegar (1996), and Mamaghani (2005). Such models provide a realistic representation of the brace cyclic axial force–deformation behavior. However, they are computationally quite expensive. Further, although computational techniques and computers are under constant development, defining each brace in a building using many finite elements is still quite cumbersome. In contrast, phenomenological models, which are based on simplified hysteretic rules that mimic the experimental cyclic axial force–deformation relationship of braces, are computationally more efficient than finite element models. Nonetheless, they usually involve numerous empirical coefficients that can be applied only to specific braces for which test data are available. Therefore, their range of application is limited. Models of this type have been developed byHigginbotham and Hanson (1976), Singh (1977), Jain and Goel (1978), and Maison and Popov (1980). On the other hand, physical theory models combine the advantages of both finite element and phenomenological models. That is, although they are relatively more universally applicable and accurate than phenomenological models, they are also computationally more efficient than finite element models. Therefore, these models are more suitable for the analytical formulation of axial force–deformation hysteretic behavior of steel braces. Physical theory models are formulated based on the physical considerations that influence the cyclic inelastic brace behavior using a simple structural system generally made of two elastic beam members and a plastic hinge. Models of this type have been developed by Nonaka (1973a,b, 1977), Zayas et al. (1981), Gugerli and Goel (1982), Ikeda and Mahin (1984), Soroushian and Alawa (1990), Remennikov and Walpole (1997), Boutros (1999), and Jin

[1]Associate Professor, Dept. of Engineering Sciences, Middle East Technical Univ., 06531 Ankara, Turkey. E-mail: mdicleli@metu.edu.tr

[2]Graduate Research Assistant, Dept. of Engineering Sciences, Middle East Technical Univ., 06531 Ankara, Turkey.

Note. Associate Editor: M. Asghar Bhatti. Discussion open until December 1, 2008. Separate discussions must be submitted for individual papers. To extend the closing date by one month, a written request must be filed with the ASCE Managing Editor. The manuscript for this paper was submitted for review and possible publication on June 22, 2007; approved on November 28, 2007. This paper is part of the ***Journal of Structural Engineering***, Vol. 134, No. 7, July 1, 2008. ©ASCE, ISSN 0733-9445/2008/7-1215–1228/$25.00.

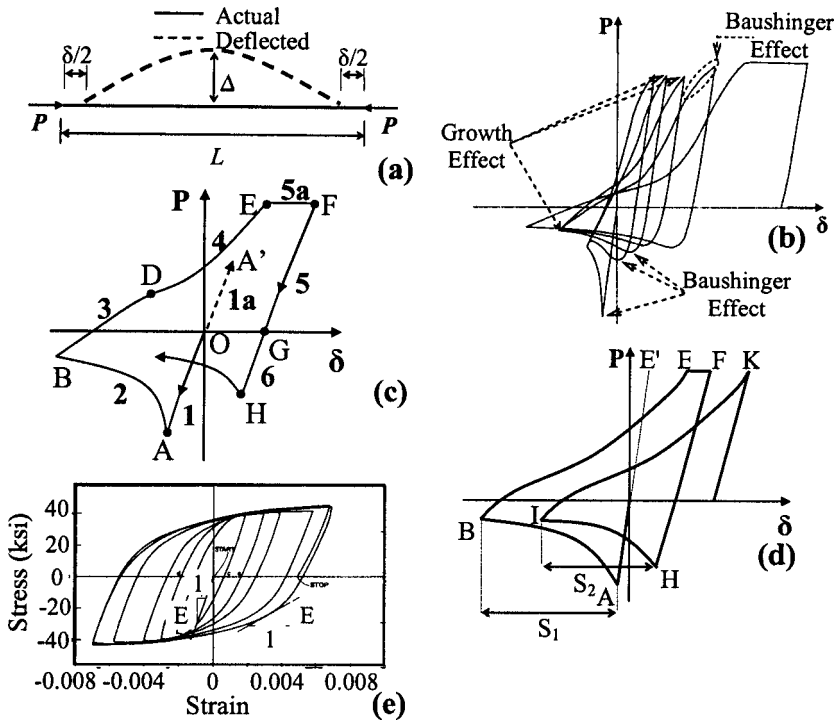

Fig. 1. (a) Deformation of brace under axial load; (b) typical brace axial force–deformation hysteresis and growth and Bauschinger effects; (c) hystereric zones; (d) demonstration of growth effect; and (e) Bauschinger effect versus tangent modulus (Black et al. 1980, with permission)

and El-Tawil (2003). However, most of the existing physical theory models are either limited by several specific empirical coefficients available only for certain brace types for the simulation of the growth and Bauschinger effects or fail to accurately simulate such effects for various brace types. In addition, most of the existing physical theory models are not capable of simulating the axial force versus transverse deformation hysteretic relationship defining the complete physical behavior of the brace. Moreover, some of the better physical theory models either involve complicated analytical functions or are very difficult to use in practice as they involve numerous implicit parameters that require extra computations to correctly define the cyclic inelastic behavior of a particular brace. Therefore, a simple physical theory model that addresses all the limitations stated previously is required.

Accordingly, this study presents a simple, yet efficient and relatively more broadly applicable physical theory model that can be used to simulate the complex inelastic cyclic axial force–axial displacement and axial force–transverse displacement relationship of steel braces. Different than many existing physical theory models, the development of the model presented in this study is based on unit dummy load method (Popov 1999) and a realistic representation of the deformed geometry of the brace incorporating second-order effects as well as the moment axial force interaction relationship of the brace cross section. Further, the analytical equations of the proposed model are simple, explicit functions of the geometric, structural, and material properties of the brace. The growth and Baushinger effects are incorporated in the model using some dimensionless semiempirical terms, which are functions of all the brace properties. Therefore, in the proposed model, the growth and Bauschinger effects are automatically adjusted as functions of the brace properties. This makes the proposed model relatively easier to use and more broadly applicable to braces with different properties. Although the model is developed for braces with pin ended connections, it may be used for braces with other end conditions using the effective length concept. Local buckling and low cycle fatigue effects are kept beyond the scope of this study.

Hysteretic Behavior of Steel Braces

General Aspects of Brace Hysteretic Behavior

The behavior of steel braces is commonly expressed in terms of an axial load, P, an axial displacement, δ, and a transverse displacement, Δ, at the vertex of the deformed brace (at the midlength of the pin ended brace) as shown in Fig. 1(a). A typical hysteresis loop of a steel brace is shown in Fig. 1(b). To study the inelastic cyclic behavior of steel braces, the axial force–deformation hysteresis can be broken into six main zones as shown in Fig. 1(c). The definition of these zones is closely related to the physical interpretation of the behavior.

In Zone 1, the brace is compressed in the linearly elastic range along Segment O–A. Due to the initial imperfections within the brace, second-order moments are generated under the applied axial load and the brace deflects transversely as demonstrated in Fig. 1(a). At a critical value of transverse displacement of the brace, the second-order moment ($P \times \Delta$) at the vertex of the deformed brace will be equal to its plastic moment capacity. At this point, the buckling load (Point A) is reached. Zone 2 is dominated by the inelastic bending of the brace due to the $P \times \Delta$ moment induced by the compressive axial load, P. Additional increases in the axial displacement results in larger transverse displacement, Δ, and a larger second-order moment at the midlength of the brace. This results in a drop in the axial force resistance of the brace along Segment A–B due to the moment–axial force interaction effects. This zone is characterized by very large lateral deflections at the midlength of the brace and by a plastic hinge in

the center region of the brace formed at buckling. Zone 3 corresponds to elastic unloading and tension loading of the brace. The slope of this zone is much smaller than that of Zone 1 due to the large permanent lateral deflection at the midlength of the brace, which results in a kinked, rather than a straight, member. Hence, the second-order effects dominate the elastic behavior within Zone 3. At Point D, the product of the axial tensile load and the transverse displacement again equals the plastic moment capacity of the brace. This is the starting point of Zone 4. At this point, a plastic hinge at the midlength of the brace is produced for the second time. However, within Zone 4 (D–E), the plastic hinge rotations act in the reverse direction of that of Zone 2 (A–B) and reduce the magnitude of the transverse deflection until the yield point, E, in tension is reached. At Point E, the brace is fully straightened and the axial load, P, is equal to the yield axial load, P_y. If the tensile force were removed at this point, the brace would remain essentially straight and be slightly longer than its original length due to a phenomenon called growth effect. The internal bending moment is essentially zero when Point E is reached, and any elongation beyond this point within Zone 5a (E–F) is a purely plastic uniaxial elongation. If the unloading occurs before Point E is reached, then the plastic uniaxial elongation region does not exist. Point F in Fig. 1(c) is a load reversal initiation point. Thus, Zone 5 consists of elastic unloading (F–G), where the brace elongation decreases linearly with decreasing tensile load. Within the region beyond Point G, which is described as Zone 6, the brace is compressed by axial force and buckled again at Point H. However, this bucking load is smaller than that of Point A due to Bauschinger effects and the residual kink remaining within the brace if unloading occurs before the axial yield capacity of the brace is reached at Point E. Zone 1a is present only if the initial loading cycle of the brace starts in tension. In Zone 1a, the brace is subjected to tensile loading in the linearly elastic range along segment $O-A'$ until the yield capacity of the brace is reached.

Growth Effect

Starting from the end of Zone 2 as shown in Fig. 1(c), the brace is subjected to elastic unloading and tension loading. During this process, the brace elongates gradually and straightens. Even though the brace, for several cycles, is subjected to the same magnitude of maximum tensile force, which may be less than the yield force, the axial displacement continues to increase. This causes a progressive lengthening of the brace called growth effect as shown in Fig. 1(b). Brace growth phenomenon is demonstrated in detail in Fig. 1(d). It influences the behavior of the brace within Zones 3 and 4 in the form of degradation of the brace axial stiffness. As observed from Fig. 1(d), for the first cycle, although the axial behavior of the brace excluding the transverse deformation effects is totally elastic, there is an apparent translation from Point E′, which is the axial displacement of the brace excluding the effect of brace growth, to Point E. For the second cycle, the brace growth corresponds to the distance from Point F to Point K only. Note that the distance between Points E and F is not considered as a growth effect. However, in this case, the plastic axial deformation between Points E and F cannot be fully recovered as upon unloading from Point F, the buckling of the brace takes place at Point G at an axial load level much smaller than the yield axial load level. This phenomenon, although not considered as growth effect, contributes to the permanent elongation of the brace length and can directly be considered in the formulation of the axial force–deformation hysteretic relationship of the brace as an unrecovered plastic deformation.

Baushinger Effect

The Baushinger effect is a natural property of steel that results in softening of the material stiffness (modulus of elasticity) proportional to the number of cyclic inelastic loading. To study the behavior of steel braces in relation to the Baushinger effect, Black et al. (1980) conducted cyclic axial force–deformation tests of a steel coupon taken from a wide flange steel brace made of ASTM A36 steel. The cyclic test results are shown in Fig. 1(e). As observed from Fig. 1(e), the Baushinger effect occurs following an initial cycle of yielding at negative and positive loading ranges before the next yielding is initiated. It is a function of the cyclic loading history. That is, the softening of the modulus of elasticity increases with increasing number of load reversals. For a typical brace, it is clearly observed from Figs. 1(b and e) that hysteresis Zones 3–4 and particularly Zone 6 are affected by the Baushinger effect. The Baushinger effect results in softening of the slope of Zone 3–4 and smaller buckling load capacities within Zone 6 at loading cycles following the initial one due to the progressive softening of the modulus of elasticity proportional to the number of loading cycles.

Proposed Physical Theory Model

In this section, a physical theory model is developed to enable the formulation of the cyclic inelastic behavior of steel braces within each hysteresis zone described earlier. The model is displayed in Fig. 2(a). It is composed of a straight elastic member with two transverse rigid bars of length, e, introduced at the member ends to create an initial axial load eccentricity that will produce buckling. A zero-length plastic hinge with elastic-perfectly plastic mechanical properties and with moment–axial force interaction capability is placed at the midlength of the member to simulate the post-buckling behavior of the brace. The zero length plastic hinge and elastic-perfectly plastic material behavior is intentionally chosen to obtain simple expressions defining the hysteretic behavior of the brace and to achieve computational efficiency in application to large scale problems. The initial eccentricity, e, is chosen such that when the axial load reaches the buckling load, P_b, of the brace, the reduced plastic moment capacity, M_{pr}, under the effect of the buckling load is also reached at the vertex of the deformed brace as shown in the plastic moment–axial force interaction diagram of Fig. 2(b). Beyond this point, the axial load capacity of the member constantly decreases due to the combined effects of increasing second-order moments and moment–axial force interaction as the member folds. For the model to work as intended, e must be known. The derivation of e is outlined in the next section. In the derivation of the analytical equations throughout this study, compressive loads (e.g., buckling load) and axial shortenings are assumed to be negative.

Derivation of the Initial Eccentricity (e) for the Model

For the derivation of e, it is assumed that the deformed shape of the brace shown in Fig. 2(a) prior to buckling can be approximated by a sinusoidal function of the form given in Eq. (1). From Fig. 2(a), the transverse displacement, $\Delta(x)$, at a location, x, from the left end of the brace can be expressed in the following form:

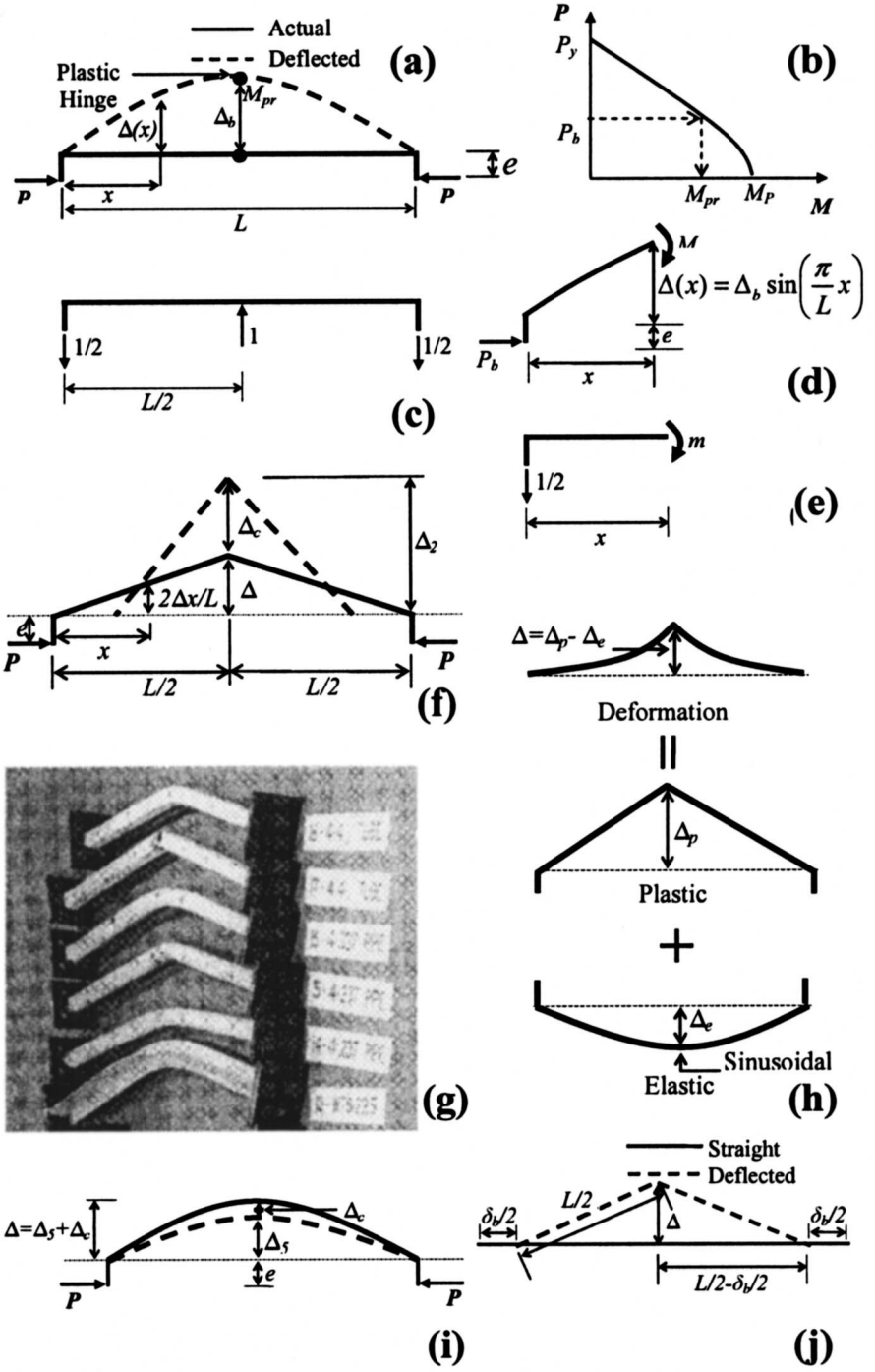

Fig. 2. (a) Deformed shape of the brace in Zone 1; (b) typical plastic moment–axial force interaction relationship for a brace; (c) application of unit dummy load; (d) free body diagram of the deformed brace under axial load to the left of the section taken at x; (e) free body diagram of the brace under unit dummy load to the left of the section taken at x; (f) deformed shape of the brace in Zone 3; (g) deformed shape of braces after the completion of testing (Black et al. 1980, with permission); (h) deformed shape and plastic and elastic deformation components of the brace in Zone 5; (i) deformed shape of the brace in Zone 6; and (j) kinematical relationship between the axial and transverse deformation of the brace

$$\Delta(x) = \Delta_b \sin\left(\frac{\pi}{L}x\right) \tag{1}$$

$$\Delta_b = 2\int_0^{L/2} \frac{Mm}{EI}dx \tag{2}$$

where Δ_b=transverse displacement at the vertex of the deformed brace at buckling. Δ_b, can be calculated using the unit dummy load method as follows (Popov 1999):

where E and I=the modulus of elasticity and moment of inertia about the buckling axis of the brace, respectively; M=second-order moment at buckling; and m=moment due to the unit

dummy load applied at the location and in the direction of the displacement to be calculated as shown in Fig. 2(c). From the free body diagrams in Figs. 2(d and e), M and m are expressed as

$$M = -P_b\left[e + \Delta_b \sin\left(\frac{\pi}{L}x\right)\right] \tag{3}$$

$$m = \frac{x}{2} \tag{4}$$

Substituting the values of M and m from Eqs. (3) and (4) into Eq. (2), integrating and rearranging the ensuing equation, Δ_b, is obtained as

$$\Delta_b = -\frac{L^2 P_b}{8EI\left(1 + \frac{P_b L^2}{\pi^2 EI}\right)}e \tag{5}$$

When the axial load is equal to the buckling load, the second-order moment at the vertex of the deformed brace element is equal to the reduced plastic moment, M_{pr}, of the brace. Accordingly, from Fig. 2(a) the following expression is formulated:

$$-P_b(e + \Delta_b) = M_{pr} \tag{6}$$

Substituting Eq. (5) into Eq. (6) and solving for e, the following expression is obtained:

$$e = -\frac{M_{pr}}{P_b\left(1 - \frac{L^2 P_b}{8EI\left(1 + \frac{L^2 P_b}{\pi^2 EI}\right)}\right)} \tag{7}$$

Note that in the previous equations, P_b needs to be taken as negative as it is an axial compressive load. This will yield a positive value for Δ_b and e. Further, the calculated e's for braces taken from the tests of Black et al. (1980) are found to be very small, ranging between 0.7 and 12 mm. Thus, the effect of e on the analytical formulations of the brace hysteretic behavior other than the simulation of buckling behavior is negligible.

Outline of the Analytical Formulations of Hysteresis Zones

Using the model described earlier, the brace axial force versus transverse displacement at the vertex of the deformed brace and axial force versus axial displacement relationships are formulated for each one of the hysteresis zones defined earlier. The formulations of the hysteretic behavior of the brace employ: (1) a large displacement analysis procedure based on an assumed deformed geometry of the brace to incorporate the second-order effects; (2) plastic moment versus axial force interaction relationship for the brace cross section combined with the estimated second order effects to simulate the buckling and postbuckling behaviors of the brace; (3) the kinematical relationship between the axial and transverse deformations of the brace; (4) elastic axial force versus displacement relationship of the brace; and (5) available experimental data to obtain dimensionless semiempirical relationships for the simulation of growth and Bauschinger effects.

In the following sections analytical equations are derived to describe the axial force versus transverse displacement relationships of the brace for each one of the hysteresis zones defined earlier. Following this, the kinematical relationship between the transverse and axial deformations of the brace is developed. Then, the total axial displacement of the brace as a function of the applied axial load is formulated for each one of the hysteresis zones. At the end, the analytically obtained hysteresis loops are verified with the experimental results of Black et al. (1980) and Goggins et al. (2006).

Axial Force versus Transverse Displacement of the Brace

In this section, analytical equations are derived to define the relationship between the axial force and the transverse displacement, Δ, at the vertex of the deformed brace for each one of the hysteresis zones defined earlier.

Formulation of the Δ–P Relationship for Zone 1

Zone 1 [Segment O–A, in Fig. 1(c)] is associated with the initial compressive loading of a brace, which approaches the buckling load at point A. For this elastic range, the deformed shape of the brace is assumed to be sinusoidal of the form given in Eq. (1) and described in Fig. 2(a). Accordingly, the transverse displacement, Δ, of the brace as a function of the applied axial load, P, can be determined following a procedure similar to that used for the calculation of e. Thus, substituting P in place of P_b in Eq. (5), the transverse displacement, Δ, of the brace for any applied axial load level can be obtained as follows:

$$\Delta = -\frac{L^2 P}{8EI\left(1 + \frac{PL^2}{\pi^2 EI}\right)}e \tag{8}$$

Formulation of the Δ–P Relationship for Zone 2

Zone 2 [Segment A–B, in Fig. 1(c)] is dominated by the inelastic bending of the brace due to the rotation of the plastic hinge formed at the vertex of the deformed brace at buckling. To satisfy static moment equilibrium, the second-order moment generated by the compressive axial load, P, must be equal to the reduced plastic moment capacity, M_{pr}, at the vertex of the deformed brace [Fig. 2(a)] regardless of the deformed shape of the brace. Thus,

$$-P(\Delta + e) = M_{pr} \tag{9}$$

From Eq. (9), Δ is obtained as follows:

$$\Delta = -\frac{M_{pr}}{P} - e \tag{10}$$

Note that in Eq. (10), the plastic moment versus axial force interaction relationship for the brace cross section must be substituted in place of M_{pr}. For instance for a steel brace made of a pipe section, M_{pr} is expressed as

$$M_{pr} = M_p \cos\left[\frac{\pi}{2}\left(\frac{|P|}{P_y}\right)\right] \tag{11}$$

where M_p=plastic moment capacity of the section at P=0. M_{pr} versus P relationships for various brace sections are developed as part of this study but are not presented due to space limitations. However, similar relationships are available in Bruneau et al. (1998).

Formulation of the $\Delta-P$ Relationship for Zone 3

Zone 3 is associated with the elastic unloading of the brace. The deformed shape of the brace within this unloading stage is approximated by two straight lines as demonstrated by the solid line sketch in Fig. 2(f). Actually, tests conducted by Black et al. (1980) confirm that braces generally deform in the form of two nearly straight line segments beyond buckling as illustrated in Fig. 2(g). This is mainly due to the severe plastic rotations at the vertex of the deformed brace element throughout Zone 2 generating very large transverse plastic displacements compared to those due to the elastic deformations of the brace. The sketch with the thick dashed line in Fig. 2(f) represents the deformed shape of the brace at the end of Zone 2, whereas the solid line sketch represents the deformed shape of the brace when the compressive axial load is dropped to a lower magnitude upon unloading or reversed to a tensile loading. In Fig. 2(f), Δ_2=transverse displacement at the vertex of the deformed brace at the end of Zone 2; Δ_c=change in the transverse displacement due to unloading or reversal to tensile loading from an axial load level P_2 at the end of Zone 2 to an axial load level P; and Δ=transverse displacement at the vertex of the deformed brace within Zone 3 at an axial load level P. From the geometry of the deformed brace shown in Fig. 2(f), Δ is expressed as

$$\Delta = \Delta_2 - \Delta_c \tag{12}$$

The displacement Δ_2 at the end of Zone 2 is known. If Δ_c is calculated and substituted in Eq. (12), the $\Delta-P$ relationship for Zone 3 can be obtained. Δ_c can be calculated using the unit dummy load method given in Eq. (2). For this purpose, the second-order moment, M, due to the change in the axial load level, $P-P_2$ and the unit dummy load moment, m, given in Eq. (4) need to be substituted in Eq. (2). Based on the deformed geometry of the brace given in Fig. 2(f) and Eq. (12), the second-order moment due to the change in the axial load level, $P-P_2$ is expressed as follows:

$$M = \left[e + \frac{2(\Delta_2 - \Delta_c)}{L} x \right] (P - P_2) \tag{13}$$

Substituting Eqs. (4) and (13) into Eq. (2), integrating and rearranging the ensuing equation, Δ_c is obtained as

$$\Delta_c = \frac{1.5e + \Delta_2}{\dfrac{12EI}{(P - P_2)L^2} + 1} \tag{14}$$

Substituting Eq. (14) into Eq. (12), the $\Delta-P$ relationship for Zone 3 is obtained as follows:

$$\Delta = \Delta_2 - \frac{1.5e + \Delta_2}{\dfrac{12EI}{(P - P_2)L^2} + 1} \tag{15}$$

Formulation of the $\Delta-P$ Relationship for Zone 4

In this zone, unlike Zone 3, the behavior of the brace is plastic. To satisfy static moment equilibrium, the second-order moment generated by the tensile axial load, P, must be equal to the reduced plastic moment capacity, M_{pr}, at the vertex of the deformed brace [Fig. 2(a)] regardless of the deformed shape of the brace. Thus

$$(\Delta + e)P = M_{pr} \tag{16}$$

Solving for Δ from Eq. (16)

$$\Delta = \frac{M_{pr}}{P} - e \tag{17}$$

Note that if the tensile axial force is equal to the yield axial force, P_y, at the end of Zone 4, the reduced plastic moment capacity, M_{pr}, of the brace must become zero due to the moment–axial force interaction relationship shown in Fig. 2(b). Thus, the second-order moment must also be equal to zero to satisfy the static moment equilibrium presented analytically in Eq. (16) when $P=P_y$. However, the presence of e in Eq. (16) makes this impossible. For this reason, e must be multiplied by a factor that makes it gradually approach zero at the yield axial load level of the brace. Accordingly, Eq. (17) is modified to satisfy static equilibrium at the yield axial load level as follows:

$$\Delta = \frac{M_{pr}}{P} - e\left(\frac{P_y - P}{P_y - P_3} \right) \tag{18}$$

where P_3=axial tensile load at the end of Zone 3.

Formulation of the $\Delta-P$ Relationship for Zone 5a

At the end of Zone 4, based on Eq. (18), if $P=P_y$, then $\Delta=0$ (i.e., the brace becomes straight). At this stage the brace has reached its axial yield capacity and the brace hysteretic behavior is now described by Zone 5a where $\Delta=0$ and $P=P_y$.

Formulation of the $\Delta-P$ Relationship for Zone 5

In Zone 5, the brace is unloaded elastically. In the development of $\Delta-P$ relationship for this zone, it is assumed that the unloading occurs at the end of Zone 4 where $P<P_y$. Consequently, the transverse displacement at the vertex of the deformed brace is not equal to zero. Obviously, if the unloading occurs within Zone 5a, then $\Delta=0$ for all the range of axial loads within Zone 5.

At the end of Zone 4, where the brace is subjected to axial tensile load, the deflection of the brace decreases to such an extent that the elastic deflections due to second-order effects become relatively significant in relation to the plastic deflections due to the rotation of the plastic hinge at the vertex of the deformed brace. Consequently, within Zone 5 the deformed shape of the brace becomes the shape shown in Fig. 2(h). The deformed shape of the brace is assumed to consist of a plastic and an elastic part as shown in Fig. 2(h). The plastic part is approximated by two straight line segments whereas the elastic part is approximated by a sinusoidal shape of the form given in Eq. (1). The transverse displacements at the vertex of the plastic and elastic parts are Δ_p and Δ_e, respectively. From Fig. 2(h), the transverse deflection, Δ, is expressed as

$$\Delta = \Delta_p - \Delta_e \tag{19}$$

Based on the previous equation, the transverse displacement, Δ_4, at the vertex of the deflected brace at the end of Zone 4 (or beginning of Zone 5) is expressed as

$$\Delta_4 = \Delta_{p4} - \Delta_{e4} \tag{20}$$

where, Δ_{p4} and Δ_{e4}=plastic and elastic transverse displacements at the vertex of the deformed brace at the end of Zone 4, respectively. Note that at the end of Zone 4, Δ_4 is known [i.e., obtained from Eq. (18)]. Both Δ_{p4} and Δ_{e4} are required for the formulation of the $\Delta-P$ relationship for Zone 5.

The elastic transverse displacement, Δ_{e4}, at the end of Zone 4 where $P=P_4$ can be calculated using the unit dummy load method presented in Eq. (2). For this purpose, the second-order moment, M, due to the applied axial load, P_4 and the unit dummy load moment, m, given in Eq. (4) need to be substituted in Eq. (2). In relation to Fig. 2(h), M is expressed as

$$M = M_{p4} - M_{e4} \tag{21}$$

where M_{p4} and M_{e4}=second-order moments due to the plastic and elastic parts of the deformed shape of the brace, respectively. From Fig. 2(h), M_{p4} and M_{e4} are first formulated and then substituted in Eq. (21) to obtain M as follows:

$$M = \left[\left(e + \frac{2(\Delta_{e4} + \Delta_4)}{L}x\right) - \left(e + \Delta_{e4}\sin\left(\frac{\pi}{L}x\right)\right)\right]P_4 \tag{22}$$

Substituting Eqs. (4) and (22) into Eq. (2), integrating and rearranging the ensuing equation, Δ_{e4} is obtained as

$$\Delta_{e4} = \frac{\pi^2 L^2 P_4 \Delta_4}{L^2 P_4(12-\pi^2) + 12\pi^2 EI} \tag{23}$$

Next, substituting Eq. (23) into Eq. (20), Δ_{p4} is obtained as

$$\Delta_{p4} = \Delta_4 + \frac{\pi^2 L^2 P_4 \Delta_4}{L^2 P_4(12-\pi^2) + 12\pi^2 EI} \tag{24}$$

It is to be noted that within Zone 5, Δ_{p4} has a constant value as it is a permanent plastic displacement whereas Δ_{e4} gradually decreases as the brace is unloaded and finally becomes zero at $P=0$. This produces a residual plastic transverse displacement, Δ_{p4} at $P=0$ as observed from the test results of Black et al. (1980). Consequently, the plastic transverse displacement, Δ_{p4}, at the end of Zone 4 is equal to the residual plastic transverse displacement within Zone 5 regardless of the axial load level. That is

$$\Delta_p = \Delta_4 + \frac{\pi^2 L^2 P_4 \Delta_4}{L^2 P_4(12-\pi^2) + 12\pi^2 EI} \tag{25}$$

Note that the residual plastic displacement (kink) is partially responsible for the early buckling of the brace. Then, from Eq. (23), substituting P in place of P_4, the elastic part of the transverse displacement, Δ_e, at any axial load level is obtained as

$$\Delta_e = \frac{\pi^2 L^2 P \Delta_4}{L^2 P(12-\pi^2) + 12\pi^2 EI} \tag{26}$$

Next, substituting Eqs. (25) and (26) into Eq. (19) and rearranging, the $\Delta-P$ relationship for Zone 5 is obtained as follows:

$$\Delta = \Delta_4 + \left[\frac{P_4}{L^2 P_4(12-\pi^2) + 12\pi^2 EI} - \frac{P}{L^2 P(12-\pi^2) + 12\pi^2 EI}\right]\pi^2 L^2 \Delta_4 \tag{27}$$

Note that in Eq. (27) at $P=P_4$, $\Delta=\Delta_4$ and if $\Delta_4=0$ then $\Delta=0$. Also, as P decreases, the magnitude of Δ gradually increases due to the effect of unloading from a tensile axial load to $P=0$.

Formulation of the $\Delta-P$ Relationship for Zone 6

Within this zone, the axial compressive load is gradually increased from zero to a level where buckling is initiated again. In this zone, the buckling load capacity is less than the initial buckling load capacity defined in Zone 1. The degradation of the buckling load capacity is caused by the Baushinger effect as well as the residual transverse displacement (kink) of the brace resulting from the plastic hinge rotations during the previous cycles. The Baushinger effect degrades the initial elastic modulus E, to a smaller value E_t, with increasing the number of cycles. Therefore, in the derivation of the analytical equations to simulate the axial force–transverse deformation relationship within this zone, the effect of the residual transverse displacement at the end of Zone 5 and the Bauschinger effect in terms of a reduced modulus of elasticity, E_t (an equivalent tangent modulus) must be included. Within this zone, similar to Zone 1, the deformed shape of the brace is assumed to be sinusoidal of the form given in Eq. (1). However, the brace is assumed to be initially kinked at the middle rather than being straight due to the residual transverse displacement, $\Delta_5=\Delta_{p4}$ at the end of Zone 5 at $P=0$ as shown in Fig. 2(i). Accordingly, with reference to Fig. 2(i), the transverse displacement, Δ, at the vertex of the deformed brace is expressed as

$$\Delta = \Delta_5 + \Delta_c \tag{28}$$

where Δ_c=change in the transverse displacement of the brace due to the effect of compressive reloading starting at the end of Zone 5. The residual transverse displacement, $\Delta_5=\Delta_{p4}$, at the end of Zone 5 is known. If Δ_c is calculated and substituted in Eq. (28), the $\Delta-P$ relationship for Zone 6 can be obtained. Δ_c can be calculated using the unit dummy load method presented in Eq. (2). For this purpose, the second-order moment, M, due to the applied axial compressive load, P and the unit dummy load moment, m, given in Eq. (4) need to be substituted in Eq. (2). Based on the deformed geometry of the brace given in Fig. 2(i), the second order moment due to the applied axial load is expressed as follows:

$$M = P\left[e + (\Delta_5 + \Delta_c)\sin\left(\frac{\pi x}{L}\right)\right] \tag{29}$$

Substituting Eqs. (4) and (29) into Eq. (2), integrating and rearranging the ensuing equation, Δ_c is obtained as

$$\Delta_c = \frac{1.5e + \frac{8}{\pi^2}\Delta_5}{\frac{12E_tI}{PL^2} + 1} \tag{30}$$

Substituting Eq. (30) into Eq. (28), the $\Delta-P$ relationship for Zone 6 is obtained as follows:

$$\Delta = \Delta_5 + \frac{1.5e + \frac{8}{\pi^2}\Delta_5}{\frac{12E_tI}{PL^2} + 1} \tag{31}$$

Note that Δ_5 will produce smaller buckling loads due to the increased second-order effects. Thus, the effect of the residual kink on buckling load is taken into consideration. This zone ends when the second-order moment becomes equal to the reduced plastic moment capacity of the brace as given by Eq. (9). At this stage, the hysteretic behavior of the brace is again defined by Zone 2.

Formulation of the $\Delta-P$ Relationship for Zone 1a

Zone 1a exists only once if the initial loading cycle of the brace starts in tension rather than compression (Zone 1). In Zone 1a, the

brace is subjected to tensile loading in the linearly elastic range and $\Delta=0$ for all the range of applied axial loads.

Kinematical Relationship between the Axial and Transverse Deformation of the Brace

A brace that is subjected to compressive loading or one that has already buckled prior to tensile loading deforms transversely as demonstrated in Fig. 2(j). As a result of this transverse deformation or bending effect, the brace becomes shorter in the axial direction. To relate the axial shortening, δ_b, of the brace due to the bending effect to its transverse deformation, Δ, the deformed shape of the brace is approximated by two straight segments as illustrated in Fig. 2(j). From the geometry of the deformed brace in Fig. 2(j), using the Pythagorean Theorem, the transverse displacement, Δ, of the brace can be obtained as

$$\Delta = \sqrt{\left(\frac{L}{2}\right)^2 - \left(\frac{L}{2} - \frac{\delta_b}{2}\right)^2} \tag{32}$$

From Eq. (32), the axial displacement, δ_b, due to the bending effect is expressed as

$$\delta_b = L - \sqrt{L^2 - 4\Delta^2} \tag{33}$$

If tensile yielding has occurred at the end of Zone 4, the brace becomes fully straight in Zones 5a and 5, and as a result, $\Delta=0$. In this case, Eq. (33) automatically yields $\delta_b=0$. Accordingly, Eq. (33) is valid for all the hysteresis zones defined earlier.

Axial Force versus Axial Displacement Relationship of the Brace

In the following, analytical equations are derived to define the axial force versus axial displacement of steel braces for each one of the hysteresis zones defined earlier.

Zones 1, 2, 5, and 6

For Zones 1, 2, 5, and 6, the total axial displacement, δ_i, of the brace (within Zone i) is expressed as

$$\delta_i = \delta_{i-1} + \delta_a - \delta_b \tag{34}$$

where δ_{i-1}=axial displacement at the end of the previous zone and δ_a=elastic axial displacement. Note that in Eq. (34), δ_b is presented as a negative value, as from the deformed geometry of the brace, shown in Fig. 2(j), under compressive or tensile axial load, the axial displacement due to the bending effect is always negative. The elastic axial displacement is expressed as

$$\delta_a = \frac{PL}{AE} \tag{35}$$

where A=cross-sectional area of the brace. Next, substituting Eqs. (33) and (35) into Eq. (34), the total axial displacement, δ_i, of the brace for Zones 1, 2, 5, and 6 is obtained as follows:

$$\delta_i = \delta_{i-1} + \frac{PL}{AE} - L + \sqrt{L^2 - 4\Delta^2} \tag{36}$$

The $\Delta-P$ relationships obtained for each one of the hysteresis zones (1, 2, 5, and 6) need to be substituted in Eq. (36) to completely define the $\delta-P$ relationships for these zones.

Zones 3 and 4

Within Zones 3 and 4, the axial displacement of the brace results from the elastic axial displacement of the brace due to the applied axial force, shortening of the brace due to the bending effect and the additional axial displacement (brace growth), δ_G, due to growth effect. Accordingly, adding δ_G to Eq. (36), the total axial displacement, δ_i, of the brace for Zones 3 and 4 is obtained as follows:

$$\delta_i = \delta_{i-1} + \frac{PL}{AE} - L + \sqrt{L^2 - 4\Delta^2} + \delta_G \tag{37}$$

The axial displacement due to the growth effect will be formulated in the subsequent sections. The $\Delta-P$ relationships obtained for each one of the hysteresis Zones 3 and 4 need to be substituted in Eq. (37) to completely define the $\delta-P$ relationships for these zones.

Zone 5a

For the case where $P=P_y$, (Zone 5a), the brace is fully straight and hence, $\Delta=\delta_b=0$. Thus, the axial displacement within this zone results from the plastic axial tensile displacement, δ_p, of the brace. Thus

$$\delta_i = \delta_{i-1} + \delta_p \tag{38}$$

Zone 1a

Zone 1a is considered only once throughout the brace's axial force–displacement hysteresis if the initial loading cycle starts in tension. In this zone, the brace is subjected to tensile loading in the linearly elastic range. The total axial displacement, δ_i, of the brace is expressed as

$$\delta_i = \frac{PL}{AE} \tag{39}$$

Test Data Used to Formulate Growth and Bauschinger Effects

The test data of Black et al. (1980) is used in this study to obtain semiempirical relationships for the simulation of growth and Baushinger effects. Black et al. (1980) conducted cyclic axial reversed loading experiments on 24 structural steel braces with a wide range of cross-section geometries. Included within the 24 selected specimens were six different cross-sectional shapes; wide flanges, thin- and thick-walled square tubes, thin- and thick-walled round pipes, structural tees, and fabricated double angles, and double channels. The material for all the rolled sections, pipes, and square tubes conformed to ASTM A36, A53 Grade B, and A501 steel, respectively. In the tests, two boundaries on the possible end conditions were considered: (1) 18 of the specimens were pinned at both ends and had slenderness ratios of 40, 80, and 120; and (2) the remaining 6 specimens were pinned at one end and fixed at the other and had slenderness ratios of 40 and 80. Details of some of the specimens used for the formulations of growth and Baushinger effects are given in Table 1.

Table 1. Properties of Steel Braces from the Tests of Black et al. (1980)

Brace	Section	σ_y (MPa)	P_b (kN)	L (mm)	KL/r
1	W 8×20	278	423	3,810	120
2	W 6×25	291	1,170	1,550	40
3	W 6×20	277	899	3,070	80
4	W 6×20	277	894	3,070	80
5	W 6×20	277	676	3,070	80
6	W 6×16	308	498	2,950	120
7	W 6×15.5	345	894	1,480	40
8	2L $6\times3\frac{1}{2}\times\frac{3}{8}$	281	877	2,830	80
10	2L $4\times3\frac{1}{2}\times\frac{3}{8}$	287	432	3,810	120
11	2C 8×11.5	245	467	3,000	120
12	WT 5×22.5	272	828	2,540	80
13	WT 8×22.5	288	872	3,190	80
14	Pipe 4×0.237	327	507	3,070	80
15	Pipe 4×0.237	327	489	3,070	80
16	Pipe 4×0.357	165	387	3,010	80
17	TS 4×4×0.25	407	547	3,050	80
18	TS 4×4×0.5	565	1,210	2,760	80

Formulation of Growth Effect

Earlier research studies have revealed that (e.g., Jin and El-Tawil 2003) brace growth is directly related to the accumulated plastic strain energy, which depends on the cumulative axial plastic displacement in compression and tension. As the plastic axial displacement in compression is kinematically related to the plastic transverse displacement of the brace, the brace growth is assumed to be a function of the cumulative transverse plastic displacement in compression plus the cumulative axial plastic displacement in tension. Methods based on the cumulative plastic strain energy necessitate extra computational steps to include the growth effect in the hysteretic behavior of the braces. Consequently, in this study, the brace growth is defined as a function of the already known plastic transverse and axial displacements of the brace to facilitate its incorporation in the hysteretic behavior of the braces and to formulate it as a function of the properties of the brace so that it can be adjusted for braces with different properties.

To include the growth effect in the analytical formulations of Zones 3 and 4, the normalized brace growth, δ_{Gn}, versus normalized cumulative plastic displacement, D_c, relationships are calculated using the experimental results of the braces tested by Black et al. (1980). The normalizations are performed to obtain a more broadly applicable relationship between the brace growth and cumulative plastic displacements that is a function of the brace properties.

For this purpose, first, brace growth, δ_G, is defined as the difference between the axial displacement, δ_i, at cycle i and the axial displacement δ_{i-1}, at cycle $i-1$ excluding any plastic displacement, δ_P. The normalized brace growth, δ_{Gn}, is then defined as

$$\delta_{Gn} = \frac{\delta_G}{\delta_e} = \frac{\delta_i - \delta_{i-1}}{\delta_e} \tag{40}$$

where δ_e=elastic axial displacement calculated using an axial load range measured from the level of axial load at the end of Zone 2 (P_2), to the level of axial load, P, where the growth is measured (usually at the end of Zone 4 where $P=P_4$). Thus

$$\delta_e = \frac{(P - P_2)L}{AE} \tag{41}$$

The normalization of the growth effect using such an axial load range is performed as the brace growth influences the hysteretic curve between the end of Zones 2 and 4 as observed from Fig. 1(b).

The normalized cumulative plastic displacement, D_c, is defined as the cumulative plastic transverse deformation $(\Delta_2-\Delta_b)$ at the end of the compression cycle (Zone 2) normalized with respect to the transverse displacement, Δ_b, of the brace at the initial buckling cycle plus the cumulative plastic deformation, δ_p, in tension normalized with respect to yield axial displacement, $\delta_y=P_yL/AE$. Thus

$$D_c = \sum_i^n \left(\frac{\Delta_2 - \Delta_b}{\Delta_b} + \frac{\delta_p}{\delta_y} \right) \tag{42}$$

where n=number of cumulative cycles up to the point where brace growth is calculated. Note that Δ_b, which is given in Eq. (5) and δ_y are functions of all the properties of the brace, that is, E, I, A, L, P_y, and P_b. The relationships between δ_{Gn} and D_c for brace slenderness ratios of KL/r=40, 80, and 120 are obtained using the test data of Black et al. (1980). The $\delta_{Gn}-D_c$ relationship for braces with KL/r=80 is plotted in Fig. 3(a). The $\delta_{Gn}-D_c$ relationships for other slenderness ratios are similar. Next, a nonlinear logarithmic regression analysis procedure is employed to obtain an analytical relationship between $\delta_G$and D_c. The obtained analytical relationships for KL/r=40, 80, and 120 are given in the following equations, respectively:

$$\delta_{Gn} = 0.65 D_c^{0.04} \tag{43a}$$

$$\delta_{Gn} = 0.08 D_c^{0.57} \tag{43b}$$

$$\delta_{Gn} = 0.1 D_c^{0.35} \tag{43c}$$

[Eq. (43*b*), is plotted in Fig. 3(a) using a thick solid line]. To obtain a universal relationship between δ_{Gn} and D_c that is applicable to any slenderness ratio different than 40, 80, and 120, an analytical relationship between δ_{Gn}, D_c, and KL/r must be formulated. This could be achieved by conducting two-dimensional regression analyses of the available data. However, to decide on the type of curve fitting technique, first, the relationship between the growth factor and the slenderness ratio at different D_c values are plotted in Fig. 3(b) for D_c=10 and 100, respectively. It is observed that the relationship between δ_{Gn}, and KL/r at different D_c values are polynomial but not similar. Thus, an adaptive polynomial curve fitting technique is used to formulate δ_{Gn}, as a function of D_c and KL/r. For this purpose, δ_{Gn}, as a function of KL/r, is assumed to have the following analytical form:

$$\delta_{Gn} = a + b\left(\frac{Kl}{r}\right) + c\left(\frac{Kl}{r}\right)^2 \tag{44}$$

where a, b, and c=coefficients defining the equation. From Eq. (44) and Eq. (43), δ_{Gn} at KL/r=40, 80, and 120 is expressed in a matrix form as follows:

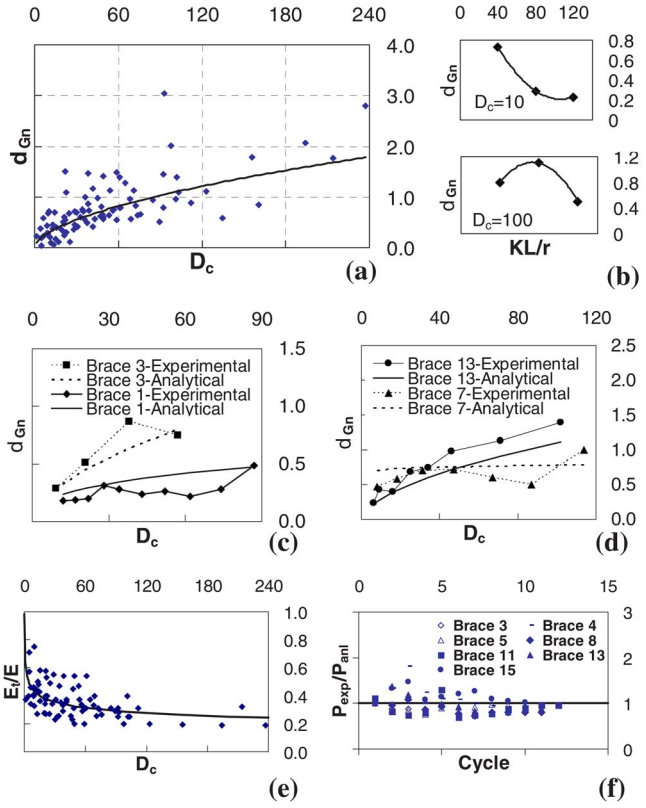

Fig. 3. (a) Normalized brace growth versus normalized cumulative displacement; (b) variation of normalized brace growth as a function of brace slenderness for $D_c=10$ and 100; (c) comparison of analytical and experimental brace growth for Braces 1 and 3; (d) comparison of analytical and experimental brace growth for Braces 7 and 13; (e) normalized tangent modulus versus normalized cumulative displacement; and (f) ratio of experimental to analytical buckling loads as a function of loading cycle number

$$\begin{pmatrix} 1 & 40 & 1{,}600 \\ 1 & 80 & 6{,}400 \\ 1 & 120 & 14{,}400 \end{pmatrix} \begin{pmatrix} a \\ b \\ c \end{pmatrix} = \begin{pmatrix} 0.65D_c^{0.04} \\ 0.08D_c^{0.57} \\ 0.1D_c^{0.35} \end{pmatrix} \tag{45}$$

From Eq. (45), the coefficients, a, b, and c are calculated as follows:

$$a = 1.95D_c^{0.04} - 0.24D_c^{0.57} + 0.1D_c^{0.35} \tag{46a}$$

$$b = (8D_c^{0.04} - 40.625D_c^{0.04} - 3.75D_c^{0.35}) \times 10^{-3} \tag{46b}$$

$$c = (31.25 \times D_c^{0.35} - 50D_c^{0.57} + 203.125D_c^{0.04}) \times 10^{-6} \tag{46c}$$

Note that the coefficients a, b, and c are functions of D_c. Thus, Eq. (44) gives an exact match to Eqs. (43) at slenderness ratios of 40, 80, and 120, respectively. From Eqs. (40), (41), and (44) the brace growth, δ_G, for Zones 3 and 4 is expressed as

$$\delta_G = \left[a + b\left(\frac{Kl}{r}\right) + c\left(\frac{Kl}{r}\right)^2 \right] \frac{(P - P_2)L}{AE} \tag{47}$$

The experimental and calculated brace growths using Eq. (47) are compared in Figs. 3(c and d) for Brace 1 ($KL/r=120$), Brace 3 ($KL/r=80$), Brace 7 ($KL/r=40$), and Brace 13 ($KL/r=80$) of Black et al. (1980). It is observed that the brace growth is simulated reasonably well for braces with various slenderness ratios and properties. Further, as δ_G is a function of D_c and D_c is a function of all the brace properties, Eq. (47) is automatically adjusted for various brace types.

Formulation of Tangent Modulus due to the Bauschinger Effect

The Bauschinger effect produces a degradation of the modulus of elasticity within the positive strain-negative stress and the negative strain-positive stress regions of the stress strain relationship of steel proportional to the cumulative plastic strain (Black et al. 1980). As the buckling load of a brace is a function of the tangent modulus of elasticity of steel; smaller buckling loads are generally obtained at subsequent cycles of the compression loading of the brace. This effect needs to be included in the analytical equations derived for Zone 6 in the form of an equivalent tangent modulus, E_t. For this purpose, as in the case of the formulation of brace growth, it is assumed that E_t is a function of D_c. Accordingly, from the experimental $P-\delta$ hysteresis curves of the braces tested by Black et al. (1980), first, experimental buckling loads, P_b, at subsequent loading cycles following the first cycle are obtained. It is noteworthy that the cycles that include the residual transverse displacement effect are excluded from the data used for obtaining E_t as a function of D_c as the reduction in the buckling capacity of a brace is also a function of the residual transverse displacement of the brace. Then, these buckling loads are substituted in Eq. (6) to calculate the transverse displacements, Δ_b at buckling. The calculated Δ_b is found to be nearly identical to the experimental ones. Next, setting the residual transverse displacement, $\Delta_5=0$, Eq. (31) is rearranged to obtain E_t as follows:

$$E_t = -\frac{P_b L^2}{I}\left(\frac{e}{8\Delta_b} + \pi^{-2}\right) \tag{48}$$

Following this, the buckling load P_b obtained from the experimental data of Black et al. (1980), Δ_b, as well as e, I, and L of the brace are substituted in Eq. (48) to calculate E_t for each loading cycle of the axial force–displacement hysteresis of the brace. Next, the ratio E_t/E of the tangent modulus to the elastic modulus is calculated and plotted as a function of D_c, for $KL/r=40$, 80, and 120. The E_t/E versus D_c relationship for braces with $KL/r=80$ is plotted in Fig. 3(e). The E_t/E versus D_c relationships for other slenderness ratios are similar. Next, a nonlinear logarithmic regression analysis procedure is employed to obtain an analytical relationship between E_t/E and D_c. The obtained analytical relationships for $KL/r=40$, 80, and 120 are given in the following equations, respectively:

$$E_t/E = 0.37D_c^{-0.12} \tag{49a}$$

$$E_t/E = 0.65D_c^{-0.18} \tag{49b}$$

$$E_t/E = 1.1D_c^{-0.26} \tag{49c}$$

[Eq. (49b) is plotted in Fig. 3(e) using a thick solid line]. Next, using a procedure similar to that used for the formulation of brace growth, E_t is expressed as a function of D_c and KL/r as follows:

$$E_t = \left[d + f\left(\frac{Kl}{r}\right) + g\left(\frac{Kl}{r}\right)^2 \right] E \tag{50}$$

where

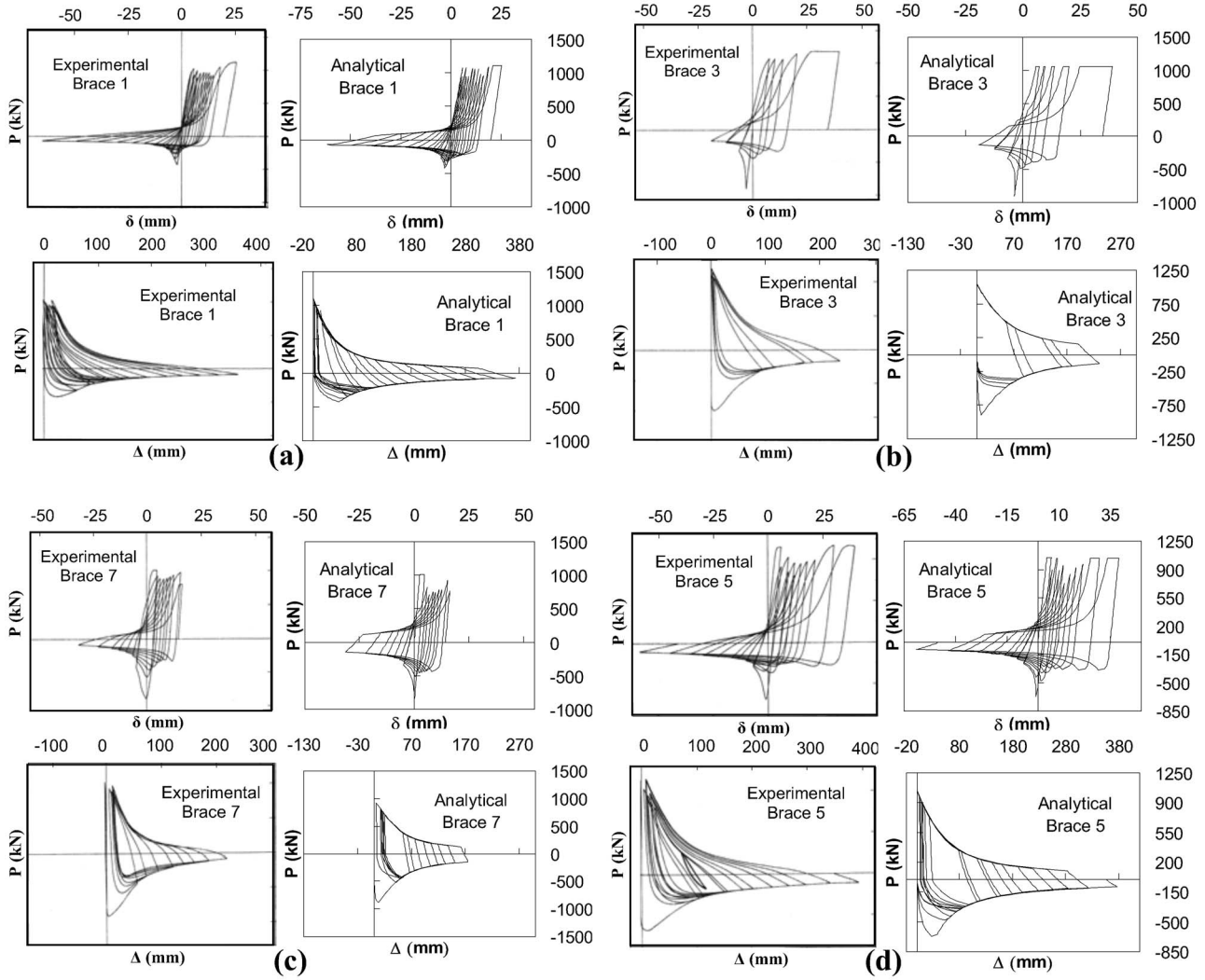

Fig. 4. Comparison of analytical and experimental axial force versus axial displacement and axial force versus transverse displacement hysteresis from the tests of Black et al. (1980) for W-section braces with various slenderness ratios (reprinted with permission): (a) Brace 1, $KL/r=120$; (b) Brace 3, $KL/r=80$; (c) Brace 7, $KL/r=40$; and (d) Brace 5, $KL/r=80$

$$d = 1.11D_c^{-0.12} - 1.95D_c^{-0.18} + 1.1D_c^{-0.26} \tag{51}$$

$$f = \left(65D_c^{-0.12} - 23.125D_c^{-0.18} - 41.25D_c^{-0.26}\right) \times 10^{-3} \tag{52}$$

$$g = \left(343.75D_c^{-0.12} - 406.25D_c^{-0.18} + 115.625D_c^{-0.26}\right) \times 10^{-6} \tag{53}$$

Subsequently, substituting Eq. (50) into Eq. (48) and solving for P_b, the analytical buckling load is obtained as follows:

$$P_b = -\frac{\left(d + f\left(\frac{Kl}{r}\right) + g\left(\frac{Kl}{r}\right)^2\right)E}{\frac{L^2}{I}\left(\frac{e}{8\Delta_b} + \pi^{-2}\right)} \tag{54}$$

The ratio of the experimental to analytical buckling loads calculated using Eq. (54) is plotted as a function of the loading cycle number in Fig. 3(f) for various braces taken from the tests of Black et al. (1980). It is observed that most of the data has a small dispersion around 1.0. This indicates a reasonably good agreement between the analytical and experimental buckling loads at various numbers of loading cycles.

Verification of the Hysteresis Model

Selection of the Braces for Verification Purposes

Eight braces from the specimens of Black et al. (1980) (Braces 1, 3, 4, 5, 7, 11, 13, and 15) and two braces from the small-scale specimens of Goggins et al. (2006) (Two 1,100 and 3,300 mm long braces with box section dimensions of $20\times20\times2$ mm and $40\times40\times2.5$ mm, respectively) were selected to verify the developed analytical model. As the effective slenderness ratio has been shown to be one of the most important parameters affecting the hysteretic behavior of braces (Black et al. 1980), the ten braces were selected to have different slenderness ratios of 40, 75, 80, 108, and 120. Included within the ten selected braces were five different cross-sectional shapes: W, WT, pipe, box, and double channel. On the basis of its common use in steel braced frame construction, the W section was chosen as a basic shape for the comparison of the analytical results with the experimental ones for different slenderness ratios of 40, 80, and 120. Therefore, five out of the ten specimens are chosen to have W sections [Braces 1, 3, 4, 5, and 7 of Black et al. (1980)]. The two small-scale box sections of Goggins et al. (2006) have slenderness ratios of

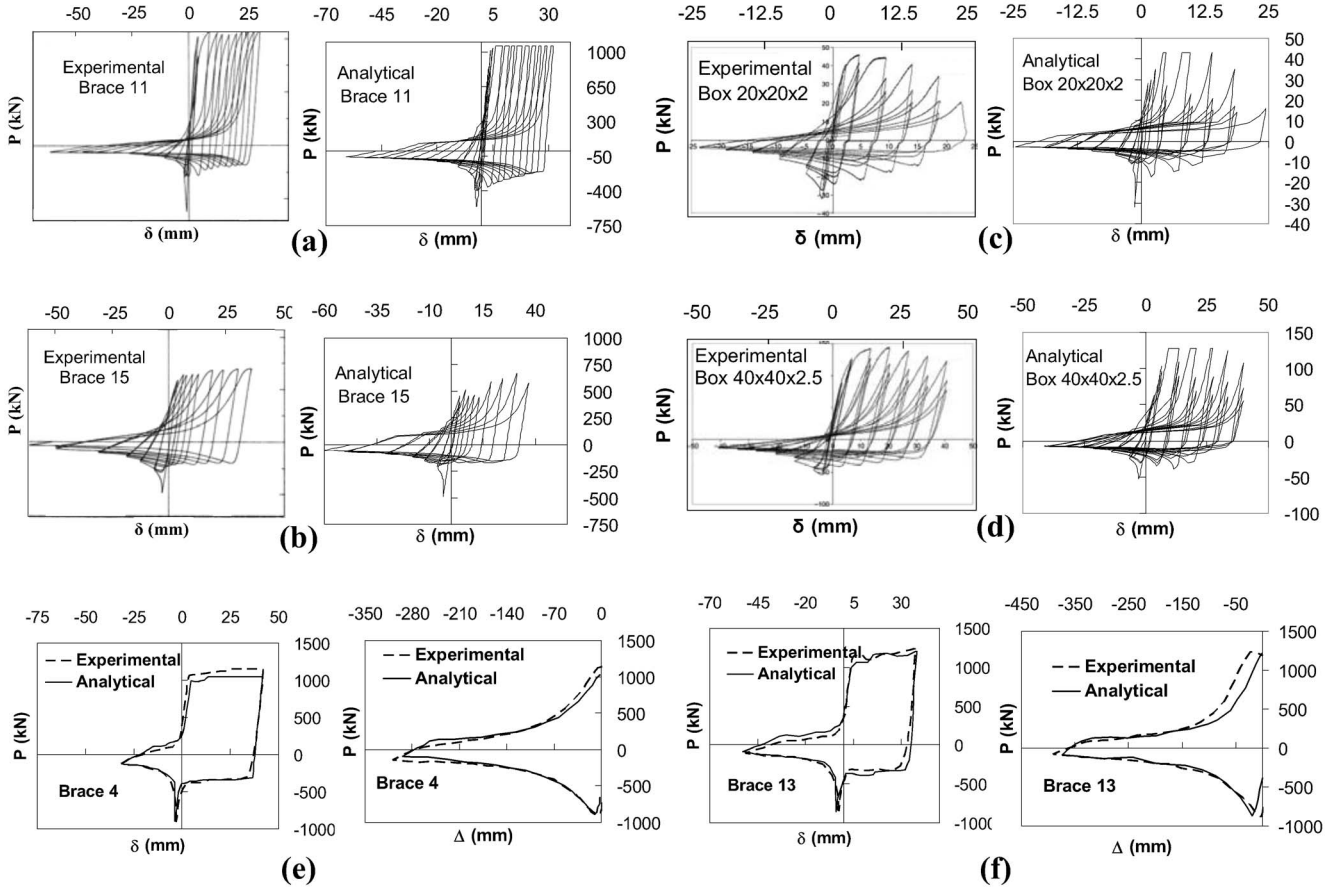

Fig. 5. Comparison of analytical and experimental axial force versus axial displacement hysteresis loops and envelopes of braces with various section shapes (reprinted with permission): (a) Brace 11, 2C 8×11.5 section of Black et al. (1980); (b) Brace 15, pipe 4×0.237 section of Black et al. (1980); (c) box $20\times20\times2$ section of Goggins et al. (2006); (d) box $40\times40\times2.5$ section of Goggins et al. (2006); (e) Brace 4, W 6×20 of Black et al. (1980); and (f) Brace 13, WT 8×222.5 of Black et al. (1980). [Material from Black et al. (1980), reprinted with permission of Earthquake Engineering Research Center. Material from Goggins et al. (2006), reprinted from *Journal of Constructional Steel Research*, 16, by J. M. Goggins, B. M. Broderick, A. Y. Elghazouli, and A. S. Lucas, "Behavior of tubular steel members under axial loading," pp. 121–131. Copyright 2006, with permission from Elsevier.]

75 and 108 and fixed end conditions. The analytical hysteresis loops of these specimens were obtained using an effective length of $0.5L$ due to their fixed end conditions. These specimens were used to demonstrate that the proposed model works for specimens different than those of Black et al. (1980) and for end conditions different than pinned.

Comparison of Hysteresis Loops

In the following the analytical axial force–axial displacement and axial force–transverse displacement hysteresis of the braces are compared with their experimental counterparts. The results are presented in Figs. 4 and 5.

Fig. 4(a) displays the analytical and experimental hysteresis loops of Brace 1 of Black et al. (1980). The brace is made of a W 8×20 section and has a slenderness ratio of 120. As observed from the plots of Fig. 4(a), the analytical hysteresis loops compare reasonably well with their experimental counterparts. Fig. 4(b) displays the analytical and experimental hysteresis loops of Brace 3. This brace is made of a W 6×20 section and has a slenderness ratio of 80. As observed from the figure, the analytical hysteresis loops closely match their experimental counterparts. Fig. 4(c) displays the analytical and experimental hysteresis loops of Brace 7. This brace is made of a W 6×15.5 section and has a slenderness ratio of 40. As observed from the plots of Fig. 4(c), the analytical hysteresis loops compare reasonably well with their experimental counterparts. Based on the above-mentioned observations, it may be concluded that the proposed hysteresis model works reasonably well for a wide range of slenderness ratios.

Fig. 4(d) displays the analytical and experimental hysteresis loops of Brace 5, which is also made of a W 6×20 section and has a slenderness ratio of 80. However, in the case of this brace, the first displacement cycle is applied in tension causing axial yielding of the specimen. Due to the Bauschinger effect, the buckling load in the first compression cycle following this tensile loading cycle is smaller than that of Brace 3, which is identical to this brace (W 6×20 and $KL/r=80$). Comparison of the analytical hysteresis loops with the experimental ones reveals that the reduction in the buckling load capacity, due to the initial tensile loading cycle (the Bauschinger effect), as well as other parts of the hysteresis loops, is analytically simulated reasonably well.

Figs. 5(a and b) display the analytical and experimental hysteresis loops of Braces 11 and 15 of Black et al. (1980). Brace 11 is made of a double C 8×11.5 built-up section and has a slen-

derness ratio of 120 and Brace 15 is made of a pipe section, O 4×0.257 and has a slenderness ratio of 80. As observed from the plots of Figs. 5(a and b), the analytical model proposed in this study simulates the cyclic inelastic behavior of the built-up and tubular braces reasonably well.

Figs. 5(c and d) display the analytical and experimental hysteresis loops of the small-scale fixed ended tubular specimens of Goggins et al. (2006), which have slenderness ratios of 75 and 108, respectively. As observed from the hysteresis loops of Fig. 5(c), although most of the tensile displacement cycles at the end of Zone 4 reach the yield point in tension, a few of these tensile cycles are stopped before the tensile axial yielding of the brace takes place. This results in a residual transverse displacement (residual kink) within the brace upon the removal of the load (i.e., at $P=0$ at the end of Zone 5). This residual kink further reduces the buckling capacity of the brace in the subsequent cycle as observed from the experimental hysteresis loop presented in Fig. 5(c). The analytical plot presented in Fig. 5(c) reveals that the proposed analytical model is capable of successfully simulating the reduction of the buckling load capacity of the brace due to the effect of the residual kink. Further, the analytical and experimental hysteresis loops compare reasonably well in spite of the much smaller scale of the specimens of Goggins et al. (2006). Consequently, it may be concluded that the proposed model seems to work for braces different than those of Black et al. (1980) and for end conditions different than pinned using an effective brace length concept.

Figs. 5(e and f) compare the analytical and experimental $P-\delta$ and $P-\Delta$ hysteresis envelopes of Braces 4 and 13 of Black et al. (1980). Brace 4 is made of a W 6×20 section and has a slenderness ratio of 80 and Brace 13 is made of a WT 8×22.5 and has a slenderness ratio of 80. As observed from the plots of Figs. 5(e and f), the analytical model proposed in this study simulates the hysteresis envelopes of W and WT sections reasonably well.

Conclusions

In this study a simple, yet an efficient physical theory model that can be used to simulate the complex cyclic inelastic behavior of steel braces is presented. The developed model incorporates simplified theoretical formulations of the inelastic behavior of steel braces. In the model, some semiempirical techniques were used to account for brace growth and degradation of buckling capacity due to the Baushinger effect. The analytical model developed in this study is verified by comparing the analytically obtained hysteresis loops with their experimental counterparts. Followings are the conclusions derived from this study:

- The analytically obtained axial force–axial displacement as well as axial force–transverse displacement hysteresis loops compare reasonably well with the experimental ones regardless of the slenderness ratio, section shape, and the end conditions of the brace.
- The model successfully accounts for brace growth and degradation of buckling capacity due to the Baushinger effect and residual kink present within the brace.
- Further, different than many existing analytical models, the semiempirical analytical equations developed to simulate the growth and Bauschinger effects are more easily and broadly applicable to steel braces with various section types and slenderness ratios. This is achieved by correlating the experimental results to the geometric and material properties of the brace.
- The developed analytical model is easier to use in practice than many existing models available in the literature as analytical equations defining the hysteretic behavior of the brace are explicit functions of the geometric and material properties of the brace.

References

Astaneh-Asl, A., and Goel, S. C. (1984). "Cyclic in-plane buckling of double angle bracing." *J. Struct. Eng.*, 110(9), 2036–2055.

Black, R. G., Wenger, W. A. B., and Popov, E. P. (1980). "Inelastic buckling of steel strut under cyclic load reversals." *Rep. No. UCB/EERC-80/40*, Earthquake Engineering Research Center, Univ. of California, Berkeley, Calif.

Boutros, M. K. (1999). "Cyclic behavior of partly plastic pinned circular tubes. II: Testing and verification of the model." *Thin-Walled Struct.*, 33(1), 69–82.

Bruneau, M., Uang, C. M., and Whittaker, A. (1998). *Ductile design of steel structures*. McGraw-Hill, New York.

Elchalakani, M., Zhao, X.-L., and Grzebieta, R. (2003). "Tests of cold-formed circular tubular braces under cyclic axial loading." *J. Struct. Eng.*, 129(4), 507–514.

Fujimoto, M., Aoyagi, T., Ukai, W. A., and Saito, K. (1972). "Structural characteristic of eccentric K-braced frames." *Transactions AIJ*, No. 195.

Goggins, J. M., Broderick, B. M., Elghazouli, A. Y., and Lucas, A. S. (2006). "Behavior of tubular steel members under cyclic axial loading." *J. Constr. Steel Res.*, 62(1-2), 121–131.

Gugerli, H., and Goel, S. C. (1982). "Inelastic cyclic behavior of steel bracing members." *Rep. No. UMEE 82R1*, Dept. of Civil Engineering, Univ. of Michigan, Ann Arbor, Mich.

Higginbotham, A. B., and Hanson, R. (1976). "Axial hysteretic behavior of steel members." *J. Struct. Div.*, 102(7), 1365–1381.

Ikeda, K., and Mahin, S. A. (1984). "A refined physical theory model for predicting the seismic behavior of braced steel frames." *Rep. No. UCB/EERC-84/12*, Earthquake Engineering Research Center, Univ. of California, Berkeley, Calif.

Jain, A. K., and Goel, S. C. (1978). "Hysteresis models for steel members subjected to cyclic buckling or cyclic end moments and buckling." *UMEE Rep. No. 78R6*, Univ. of Michigan, Ann Arbor, Mich.

Jain, A. K., Goel, S. C., and Hanson, R. D. (1978). "Hysteretic behavior of bracing members and seismic response of braced frames with different proportions." *Research Rep. No. UMEE 78R6*, Univ. of Michigan, Ann Arbor, Mich.

Jin, J., and El-Tawil, S. (2003). "Inelastic cyclic model for steel braces." *J. Eng. Mech.*, 129(5), 548–557.

Kayvani, K., and Barzegar, F. (1996). "Hysteretic modelling of tubular members and offshore platforms." *Eng. Struct.*, 18(2), 93–101.

Maison, B., and Popov, E. P. (1980). "Cyclic response prediction for braced steel frames." *J. Struct. Div.*, 106(7), 1401–1416.

Mamaghani, I. H. P. (2005). "Inelastic cyclic analysis of steel braces." *Proc., 33rd CSCE Annual Conf.*, GC-193-1–GC-193-10.

Nonaka, T. (1973a). "Elastic-plastic analysis of a bar under repeated axial loading." *Int. J. Solids Struct.*, 9(5), 569–580 (Erratum in No. 10, p. 569).

Nonaka, T. (1973b). "Erratum: Elastic-plastic analysis of a bar under repeated axial loading." *Int. J. Solids Struct.*, 9(10), 569.

Nonaka, T. (1977). "Approximation of yield condition for the hysteretic behavior of a bar under repeated axial loading." *Int. J. Solids Struct.*, 13(7), 637–643.

Popov, E. P. (1999). *Introduction to mechanics of solids*, Prentice-Hall, Englewood Cliffs, N.J.

Remennikov, A. M., and Walpole, W. R. (1997). "Analytical prediction of seismic behavior for concentrically-braced steel systems." *Earthquake Eng. Struct. Dyn.*, 26(8), 859–874.

Shaback, B., and Brown, T. (2003). "Behavior of square hollow structural

steel braces with end connections under reversed cyclic axial loading." *Can. J. Civ. Eng.*, 30(4), 745–753.
Sherman, D. R., and Erzurumlu, H. (1976). "Ultimate capacity of tubular beam-columns." *Presented at the National Structural Engineering Conf.*, ASCE, New York.
Singh, P. (1977). "Seismic behavior of braces and braced steel frames." Ph.D. thesis, Univ. of Michigan, Ann Arbor, Mich.
Soroushian, P., and Alawa, M. S. (1990). "Hysteretic modeling of steel struts: Refined physical theory approach." *J. Struct. Eng.*, 116(10), 2903–2916.
Wakabayashi, M., Matsui, C., and Mitani, I. (1977). "Cyclic behavior of a restrained steel brace under axial loading." *Proc., 6th World Conf. on Earthquake Engineering*, Vol. 11, 189–194.
Zayas, A. Z., Mahin, S. A., and Popov, E. P. (1980). "Cyclic inelastic behavior of steel offshore structures." *Rep. No. UCB/EERC-80/27*, Earthquake Engineering Research Center, Univ. of California, Berkeley, Calif.
Zayas, A. Z., Shing, P. B., Mahin, S. A., and Popov, E. P. (1981). "Inelastic structural modeling of braced offshore platforms for seismic loading." *Rep. No. UCB/EERC-81/04*, Earthquake Engineering Research Center, Univ. of California, Berkeley, Calif.